# Adaptive Feet for Quadrupedal Walkers

Manuel Giuseppe Catalano ⬤, Mathew Jose Pollayil ⬤, Giorgio Grioli ⬤, Giorgio Valsecchi ⬤,
Hendrik Kolvenbach ⬤, Marco Hutter ⬤, Antonio Bicchi ⬤, *Fellow, IEEE*, and Manolo Garabini ⬤

*Abstract*—The vast majority of state-of-the-art walking robots employ flat or ball feet for locomotion, presenting limitations while stepping on obstacles, slopes, or unstructured terrain. Moreover, traditional feet for quadrupeds lack sensing systems that are able to provide information about the environment and about the foot interaction with the surroundings. This further diminishes their value. Inspired by our previous work on soft feet for bipedal robots, we present the SoftFoot-Q, an articulated adaptive foot for quadrupeds. This device is conceived to be robust and able to overcome the limitations of currently employed feet. The core idea behind our adaptive foot design is first introduced and validated through a simplified mathematical formulation of the problem. Subsequently, we present the chosen mechanical implementation to attempt overcoming current limitations. The realized prototype of adaptive foot is integrated and tested on the compliantly actuated quadrupedal robot ANYmal together with an ROS-based real-time foot pose reconstruction software. Both extensive field tests and indoor experiments show noticeable performance improvements, in terms of reduced slippage of the robot, with respect to both flat and ball feet.

*Index Terms*—Adaptive feet, quadrupedal robots, soft foot.



Fig. 1. SoftFoot-Q, a passive adaptive foot designed for quadruped robots.

## I. INTRODUCTION

WHEN compared to wheels, although less easy to construct and control, legs have distinct advantages and can provide superior mobility and agility. Climbing obstacles,

Manuel Giuseppe Catalano and Giorgio Grioli are with the Soft Robotics for Human Cooperation and Rehabilitation, Fondazione Istituto Italiano di Tecnologia, 16163 Genova, Italy (e-mail: manuel.catalano@iit.it; giorgio.grioli@gmail.com).

Mathew Jose Pollayil and Antonio Bicchi are with the Centro di Ricerca "Enrico Piaggio," Università di Pisa, Pisa 56122, Italy, with the Soft Robotics for Human Cooperation and Rehabilitation, Fondazione Istituto Italiano di Tecnologia, Genova 16163, Italy, and also with the Dipartimento di Ingegneria dell–Informazione, Università di Pisa, Pisa 56122, Italy (e-mail: mathewjosepollayil@gmail.com; antonio.bicchi@unipi.it).

Giorgio Valsecchi, Hendrik Kolvenbach, and Marco Hutter are with the Robotic Systems Lab, ETH Zurich, 8092 Zurich, Switzerland (e-mail: giorgio.valsecchi@mavt.ethz.ch; hendrikk@ethz.ch; mahutter@ethz.ch).

Manolo Garabini is with the Centro di Ricerca "Enrico Piaggio," Pisa 56122, Italy, and also with the Dipartimento di Ingegneria dell–Informazione, Università di Pisa, 56122 Pisa, Italy (e-mail: manolo.garabini@gmail.com).

leveraging the environment for support or pushing-off, and executing dynamic maneuvers—like jumping or bounding—are just some of the notable capabilities enabled by legged locomotion [1]. Humans and animals strongly rely on the particular mechanical structure of their feet to be more stable and agile, as well as to move more flexibly and efficiently [2]. Feet are central organs that help to isolate the body from terrain irregularities by adapting themselves to features such as local ground curvature and inclination [3], [4]. This isolation property is even more relevant in the case of robots [5]. Furthermore, in living beings, the sensing abilities of the skin provide sensory inputs about foot placement and loading that are used by the central nervous system to control balance and subsequent movements. Studies suggest that sensory functions of feet are critical in controlling balance during human locomotion [6].

However, while considerable attention is given to hand design in the field of robotic end-effector development, much less focus is devoted to mechanical foot design for stable locomotion and environment exploration through sensing. A substantial effort on artificial feet design has been put only in the field of prosthetic devices to replicate the functionality of human feet and to achieve the additional aim of reaching high-level performance in traits like metabolic efficiency and comfortable daily use [7]–[9]. Energy-efficient bionic feet using elastic actuators are also proposed in [10]. Still, unfortunately, the application of advanced feet in robotics is not common at all, notwithstanding the aforementioned distinct

advantages. More details about the current trends can be found in Section II.

In this context, this article introduces the SoftFoot-Q (see Fig. 1), a robotic foot prototype for quadrupedal walkers devised to be able to increase locomotion flexibility and robustness together with the ability to sense and interact with the environment while endeavoring to limit mechanical and control complexity. The proposed design is loosely inspired by our previous work [11] and encouraged by the results of [12]. In the light of the considerations and of the differences from [11] and [12], discussed in Section IV, the contributions of the present work are the following:

1) the SoftFoot-Q, an entirely novel and robust adaptive foot, explicitly devised for quadrupedal locomotion in very challenging conditions;
2) a more complete mathematical validation of the concept;
3) an integrated low-cost and robust sensing system for haptic exploration;
4) indoor and in field validation, even on very harsh terrains, that proves effective reduction of slippage during locomotion on a state-of-the-art robotic quadruped.

In Section II, a quick review of the currently employed robotic feet and their limitations is carried out. Subsequently, Section III conducts a mathematical analysis of the influence of foot-sole shape on the stability of foot-terrain interaction, which leads to the core idea of our adaptive foot and to the choice of the foot design, explained in Section IV. In Section V, we present the mechanical implementation of our robotic foot. The particulars about its sensorization are provided in Section VI. Four of these novel foot prototypes are built and tested on the ANYmal quadruped [13], as Section VII describes in detail. Section VIII concludes this article.

## II. STATE OF THE ART

The majority of legged bipeds walk on flat feet with actuated ankles (e.g., ATLAS [14], Digit [15], HRP3 [16], HUBO [17], Nao [18], Talos [19], Toro [20], Walkman [21]) or, rarely, on very simple ball feet (e.g., Hume [22] or Mabel [23]) or on active/passive line contact feet (e.g., Cassie [24] and Mercury [25]). This is due to the fact that bipeds need to exert torques on the ground for balancing, which mostly requires actuated planar feet. Instead, multilegged systems can make use of more simplistic feet: almost all quadrupedal robots (e.g., ANYmal [13], HyQ [26], Laikago [27], MIT Cheetah [28], SpotMini [29]), employ passive ball shaped feet.

Currently employed robotic feet privilege simplicity and robustness at the cost of reducing functionality. However, there are several concepts of enhanced feet that could, in principle, improve robot performance in terms of stability and perception, but severely lack real-world validation. Most of them are adaptive devices that make use of inflatable balls or other delicate soft components that are hardly useable in harsh outdoor settings. For instance, the one presented in [30] is a flexible humanoid foot design made of a flat part with rubber pads for absorbing impacts. In [31], a mechanical realization of the lower body of the "cCub" robot is shown, but the foot sole is just a solid plate divided into two parts. A passive foot that uses an airtight bag filled with granular material was developed in [32], but the work lacks an experimental validation of the prototype on a robot. In a previous work, we also have shown how to realize a passive adaptive planar foot with sensing capabilities [33].

There are also a few adaptive foot designs that are made of actuated components: although a human-like robot foot prototype is described in [34], it is validated only by attaching it to a stationary rig and lowering it onto different surfaces. A biped foot mechanism with four spikes that modify their height according to the terrain using optical distance sensors is shown in [35]. Still, the authors themselves admit that their solution cannot be used on soft and deformable terrain such as sand or snow. A foot system made of an actuated ankle and five rigid bodies connected via passive joints is presented in [36]; however, for achieving adaptability, they focused more on an active spine and distributed control rather than the mechanics of the foot itself. Other studies on bio-mimetic concepts (e.g., [37] and [38]) implement adaptive mechanisms or mechanical intelligence in robotic feet mainly in order to maximize traction. Finally, feet that attempt to mimic the compliance and adaptability of human feet are presented in works such as [39] and [40], but these provide no significant experimental results.
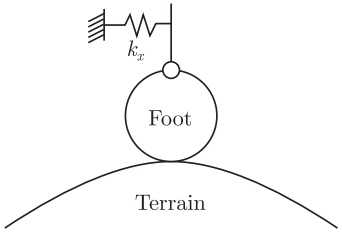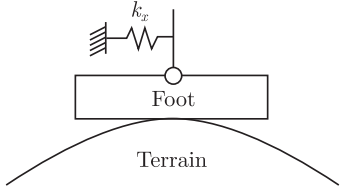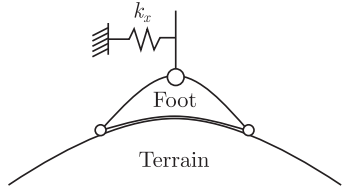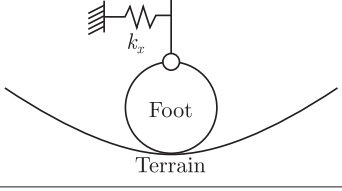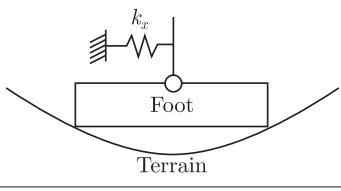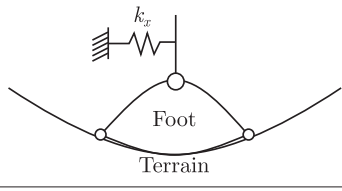
Furthermore, current robotic feet are rarely equipped with sensing devices in their soles. This goes against the knowledge that sensed data (posture, force/torque, pressure) from the feet are vital for efficient control of balancing and walking. Only a few exceptions employ expensive force/torque or pressure sensors [41], [42] or a combination of inertial measurement units (IMUs) and force/torque sensors [33] to estimate contact force or pressure.

Most of the aforementioned robotic feet have very little mechanical and functional sophistication. The limited use of advanced feet, such as mechanically adaptive feet, is likely resulting from several hindrances including the following.

1) *Mechanical complexity*—an adaptive or active foot is generally more complex with respect to a foot with rigid flat sole and might be less robust and not suitable in practice for harsh interactions.
2) *Modeling complexity*—advanced feet are usually more difficult to model and hence also more intricate to simulate.
3) *Control complexity*—novel feet designs are typically not compatible with the flat floor hypothesis [43], hence most locomotion algorithms do not apply in a straightforward way;
4) *Weight*—the need to apply and bear large loads makes active robotic feet heavy and not easily adaptable to multilegged robots and, moreover, moving a heavy mass at the tip of the leg is not at all desirable.

Despite these potential hindrances, adaptive feet can provide many advantages to locomotion, e.g., leveraging the environment for support or pushing-off, adapting to the conditions of the terrain. Another benefit is the increased perception given by the possibility of exploiting environment and objects with the robot sole for estimating surface features, textures, and friction. This allows the feet to be used to inspect the environment as

TABLE I
STABILITY ANALYSIS: THE THREE DIFFERENT FEET COMING INTO CONTACT WITH CONVEX TERRAIN

| Ball | Flat | Soft |
|---|---|---|
|  |  |  |
| $r > 0 \wedge \frac{r}{R} > 0$ | $r \to +\infty \wedge \frac{r}{R} > 0$ | $r < 0 \wedge \frac{r}{R} < -1$ |
| Unstable for low $k_x > 0$ | Stable for $k_x > 0$ | Stable even in absence of $k_x$ |
|  |  |  |
| $r > 0 \wedge -1 < \frac{r}{R} < 0$ | $r \to +\infty \wedge \frac{r}{R} < 0$ | $r > 0 \wedge -1 < \frac{r}{R} < 0$ |
| Stable for $k_x > 0$ | Stable for $k_x > 0$ | Stable even in absence of $k_x$ |

shown in [44]. With the right sensors, feet can be used as adaptive probes that are able to enhance the perception of unstructured environments through haptic reasoning, as we have shown in a previous work [45]. Especially in the case of impaired vision, visual and haptic information can be integrated to assess the shape and softness of the surroundings [46]. Hence, knowing the properties of the terrain, such as its compliance and local curvature, can considerably improve the stability of a walking robot [46]–[48].

## III. MODELING

In this section, we conduct a mathematical study of the stability properties of a generic robotic foot in relation to the shape of its sole for both the cases of locally convex and concave terrains. Therein, we purposely neglected static friction as we intended to develop a design that is inherently stable even in the absence of frictional effects. The aim of this simplified study is to roughly justify our choice of design.

Consider the simplified model of a robotic foot contacting the terrain, as shown in Fig. 2. Here, $m$ stands for the mass of the foot; $r \in \mathbb{R}$ and $R \in \mathbb{R}$ stand for the local signed radii of curvature of respectively the foot and the terrain at the contacting point. A negative value of the radii would change the shape of the foot or the terrain to be concave. The parameters $k_x$, $c_x$ and $k_y$, $c_y$ are related to the impedance of the robotic leg in the $x$ and $y$ directions, respectively. The dynamic frictional effects at the contact surface are modeled by the coefficient $c_\theta$. Let $x_p$ and $y_p$ be the reference positions of the foot and $\theta$ the Lagrangian angular coordinate of the midpoint of the foot with respect to the center of the terrain curvature. To derive the model of the foot-terrain interaction dynamics, we choose as state $\zeta = [\zeta_1 \ \zeta_2]^T = [\theta \ \dot{\theta}]^T$
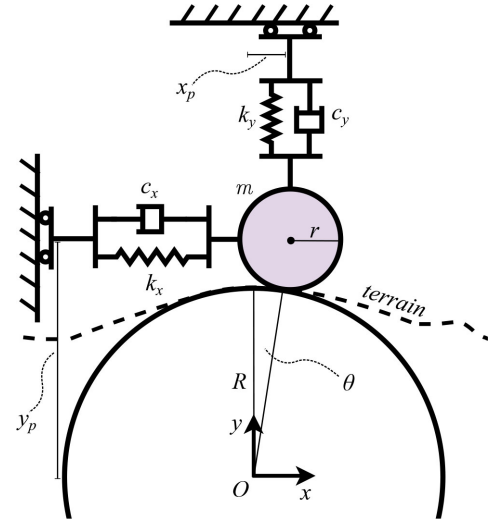


Fig. 2. Simplified 2-D model of a robotic foot contacting an uneven terrain, which is used for foot-terrain interaction stability analysis. Results are reported in Table I.

and as input $u = [u_1 \ u_2]^T = [x_p \ y_p]^T$. By employing the Lagrangian formulation, using $\theta$ as Lagrangian variable, we write the nonlinear dynamics of the foot-terrain system in the state space [49]

$$
\begin{cases}
\dot{\zeta}_1 = \zeta_2 \\
\dot{\zeta}_2 = -\zeta_2 \left[ \dfrac{(R+r)(c_x R \cos^2 \zeta_1 + c_y R \sin^2 \zeta_1) + c_\theta}{m(R+r)^2} \right] \\
\qquad + \dfrac{\sin(2\zeta_1)(k_y - k_x)}{2m} \\
\qquad + \begin{bmatrix} \dfrac{k_x \cos \zeta_1}{m(R+r)} & \dfrac{-k_y \sin \zeta_1}{m(R+r)} \end{bmatrix} u.
\end{cases}
\tag{1}
$$

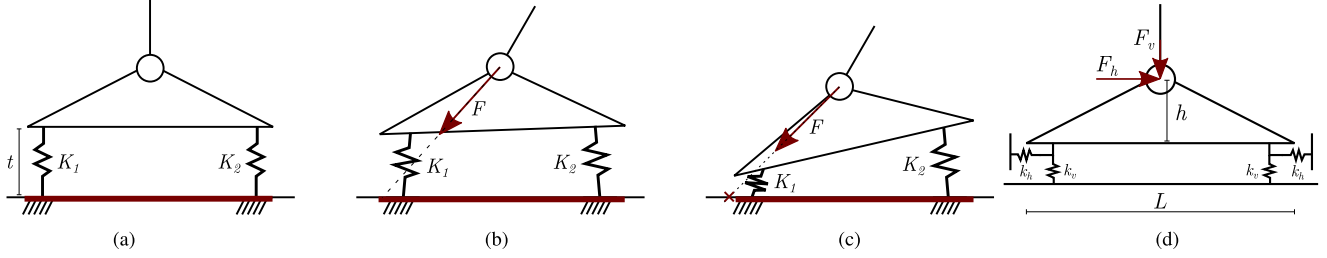Fig. 3. Simplified model of a robotic foot with elastic element under the sole. (a) Foot with rubber sole of thickness t. The support area is highlighted in red on the ground. Deformation and projection of a same resultant force $F$ in the two cases of rubber sole with (b) high and (c) low stiffness. (d) Simplified 2-D model of a foot with soft material under the sole.

Linearizing (1) about the feasible equilibrium of the system, which is given by $\zeta_{eq} = [\zeta_{1_{eq}} \ \zeta_{2_{eq}}]^T = [0 \ 0]^T$, $u_{eq} = [u_{1_{eq}} \ u_{2_{eq}}]^T = [0 \ \bar{y}_p]^T$, we obtain

$$\dot{\xi} = \begin{bmatrix} 0 & 1 \\ -\eta_1 & -\eta_2 \end{bmatrix} \xi + \begin{bmatrix} 0 & 0 \\ \frac{k_x}{m(R+r)} & 0 \end{bmatrix} v \quad (2)$$

where $\xi$ and $v$, respectively, stand for state and input perturbations in a neighborhood of the equilibrium. The parameters $\eta_1$ and $\eta_2$ are

$$\eta_1 = \frac{k_x(R+r) + k_y(\bar{y}_p - R - r)}{m(R+r)}, \quad \eta_2 = \frac{c_\theta + c_x R(R+r)}{m(R+r)^2}. \quad (3)$$

If we assume that both the environment and the robotic foot are able to withstand the vertical interaction force given by $|F_y| = k_y|(\bar{y}_p - R - r)|$, the foot-terrain system is at equilibrium $\forall \bar{y}_p < R + r$, which guarantees contact of the foot with the ground.

The stability of the nonlinear system about the equilibrium, as studied in [49], taking into account that $m > 0$, $|F_y| = k_y|(\bar{y}_p - R - r)|$ and $R \neq -r$, is granted by

$$k_x > (R+r)^{-1}|F_y|. \quad (4)$$

Condition (4) yields some interesting conclusions. If $R > 0$, the terrain is locally convex at the contact point (cases illustrated in the first row of Table I). In this case, for both the ball and flat feet, a positive bound on the horizontal stiffness $k_x$ of the robotic leg is required for the stability of the system. Instead, for an adaptive foot, the bound on $k_x$ is a negative value, hence the system is always stable for any physically possible value of horizontal stiffness of the leg. Instead, if the terrain is concave at the contact ($R < 0$), all feet exhibit an interaction stabilizing behavior (second row of Table I). Consequently, if either the foot or the terrain has a concave shape, the foot-terrain interaction is locally stable. Thus, a foot that can become convex or concave using its capacity to conform to the shape of the terrain (third column of Table I) has the property of inherently stabilizing the interaction dynamics.

This highlights how the curvature of the robotic sole plays a critical role in the stability of the sole-terrain interaction. The more the curvature of the sole adapts to the contact surface, the more the contact dynamics with the foothold is stable, even in the absence of static friction at the contact. Frictional phenomena,

on the other hand, can always aid in and improve the stability of the interaction in all of the three cases shown in Table I.

The desired property of being able to adjust the sole to the curvature of the terrain can be implemented on a robotic foot in at least two ways: 1) by inserting a thick, soft layer under the sole; or 2) by mechanically designing the foot to have an adaptable sole. The former case, also analyzed in [11], presents some shortcomings, as illustrated in the thought experiment in Fig. 3. A soft component under the sole can be modeled with two springs of equal stiffness $K_1 = K_2$. When a nonvertical force acts on the ankle, it will cause the foot to incline in one direction and potentially tilt if the stiffness of the springs is below a given threshold, since the projection of the force might lay outside the support surface [see Fig. 3(c)]. The higher the thickness $t$ of the soft component below the sole, the higher also the pivot point and the more the chance for the foot to become unstable, as the resulting moment is bigger. Moreover, the physical limits on ankle motion and the available control torque by the foot lead to lower bounds on the stiffness of soft components under the sole: this has been extensively discussed in [11].

An additional reason against a foot with soft layer sole is found by studying the balance of forces on the simple model shown in Fig. 3(d). The equilibrium of vertical forces is as follows:

$$F_v = k_v \delta_{v_1} + k_v \delta_{v_2}. \quad (5)$$

Here, $\delta_{v_1}$ and $\delta_{v_2}$ are the displacements of the left and right vertical springs respectively. If we assume that the ankle joint does not transmit any torque along its axis from the leg to the foot (for instance, it might be a revolute joint), the equilibrium of moments can be expressed approximately as

$$0 = -F_h h - k_v \delta_{v_1} \frac{L}{2} + k_v \delta_{v_2} \frac{L}{2}. \quad (6)$$

From (5) and (6), the vertical displacements of the springs can be computed as

$$\delta_{v_1} = \frac{1}{2} \left( \frac{F_v}{k_v} - \frac{2F_h h}{k_v L} \right), \quad \delta_{v_2} = \frac{1}{2} \left( \frac{F_v}{k_v} + \frac{2F_h h}{k_v L} \right) \quad (7)$$

and the difference between the displacements of the two vertical springs can be directly found from (6) as

$$\delta_v = \delta_{v_2} - \delta_{v_1} = \frac{2F_h h}{k_v L} = 2pF_h. \quad (8)$$
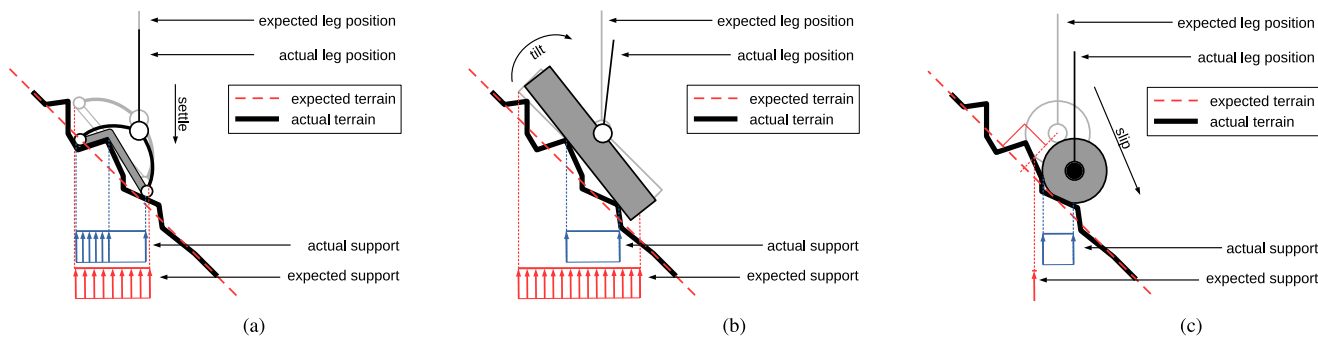
Fig. 4.    Three different kinds of feet: (a) adaptive foot; (b) flat foot; (c) ball foot. coming into contact with an irregular slope. Differences between expected contact and actual contact manifest in terms of different foot position and orientation, different support polygon, and different distribution of pressure.

As expected, foot stability depends on the variable $p = \frac{h}{k_v L}$, which is a combination of the height of the pivot point and the softness of the sole. It is noteworthy, from (7) and (8), that $p$ has particular relevance in helping choose the correct design for a stable adaptable foot. A high value of $p$ leads to an easier tilting, increasing the chance of instability of the design, and so a low value of $p$ is desirable. As a consequence, ideally, the height of the joint should be kept low, the base wide, and the sole as stiff as possible. However, as there are usually limitations on the geometric size of the foot (on $h$ and $L$), for the architecture to be stable, the sole stiffness $k_v$ should be relatively high. Therefore, it becomes clear that the thickness of rubber-like elements under the sole should be kept at a minimum. This motivates our choice of implementing the alternative solution of a mechanically adaptive sole.

## IV.  ADAPTIVE FEET: IDEA

Based on the results of Section III, we propose a passive-adaptive foot with a mechanically deformable and adaptable sole. As illustrated in the simplified drawing in Fig. 4(a), the sole itself of our robotic foot is deformable without any thick, soft part under the base. In this manner, the prototype is able to adapt to the shape of the ground while minimizing the chance of instabilities due to the deformation of elastic elements under the base of the foot.

As illustrated in Fig. 4(a), the intended behavior of our foot design when approaching the soil is to act as a rope in a tension state. In particular, as the foot approaches the ground, parts of the sole will start touching some of the peaks of the ground. In this condition, a flat foot would stop as soon as there are enough contact points to limit the motion (assuming a sufficient amount of friction, this would happen with two contact locations in a planar example as in Fig. 4(b), or three not aligned contacts in 3-D space). Instead, a ball foot might contact the terrain on a tiny surface (a point in the worst case), increasing the chance of slippage, as Fig. 4(c) shows. The adaptive foot, on the other hand, can continue to move down, "settling" its position until the flexible sole becomes sufficiently tense. In performing this motion, the foot would wrap around the convex hull of a subset of the points on the ground. The usage of such an adaptive foot could also have the effect of increasing the size of the support

area unless the terrain surface is even and perfectly flat: in such an ideal case, the flat foot would surely maximize the contact area. However, in real-world situations, surfaces are irregular, and hence adaptive feet have more chance to lead to a larger support area.

Our design, extensively explained in Section V, is loosely derived from the one presented [11] (SoftFoot), which has been later tested on the HRP-4 biped in [12]. However, the prototype presented therein is meant to be a humanoid adaptive foot. So, it combines the design of an adaptive sole with fingers and a system to implement a windlass-like mechanism, which is a function of the anatomy of the base of the foot that helps in maintaining stability when the foot is still in contact, but the heel rises from the ground [50]. In [11], the authors also state that the SoftFoot needs further optimization and field validation. However, the prototype has not been modified in [12], except for a connection interface, and no extensive validation has been carried out: the authors themselves admit that the presented results are simply a proof of concept to demonstrate the employability of their adaptive foot on the HRP-4 robot. In both [11] and [12], the adaptive foot has never been tested outdoors on harsh terrains.

In contrast, the design proposed in the present work is entirely new and is explicitly devised for being used on quadrupedal robots in very harsh environments. Since the SoftFoot is "a mechanical architecture that translates in a feasible engineered complexity the behavior of a human foot," a complete redesigning was required for reducing unnecessary sophistication and increasing robustness. Additionally, the SoftFoot has dimensions and weight that are in line with the state-of-the-art humanoid bipeds. Hence, it cannot be employed on the small legs of quadrupedal robots.

In accordance with the above, the main design goals of SoftFoot-Q were lightness, size reduction, robustness, and adaptability. Our foot preserves from the SoftFoot only the two arch structure together with the idea of a mechanically compliant sole that leads to a stiffening-by-compression behavior. SoftFoot-Q does not present the windlass-like mechanism anymore, as we wished to reduce the complexity of the design. The number of components are also considerably lower than SoftFoot, which also aided in ensuring a relatively low weight of the prototype. Moreover, the new foot is enhanced with an extra degree of freedom in order to extend the adaptation of the
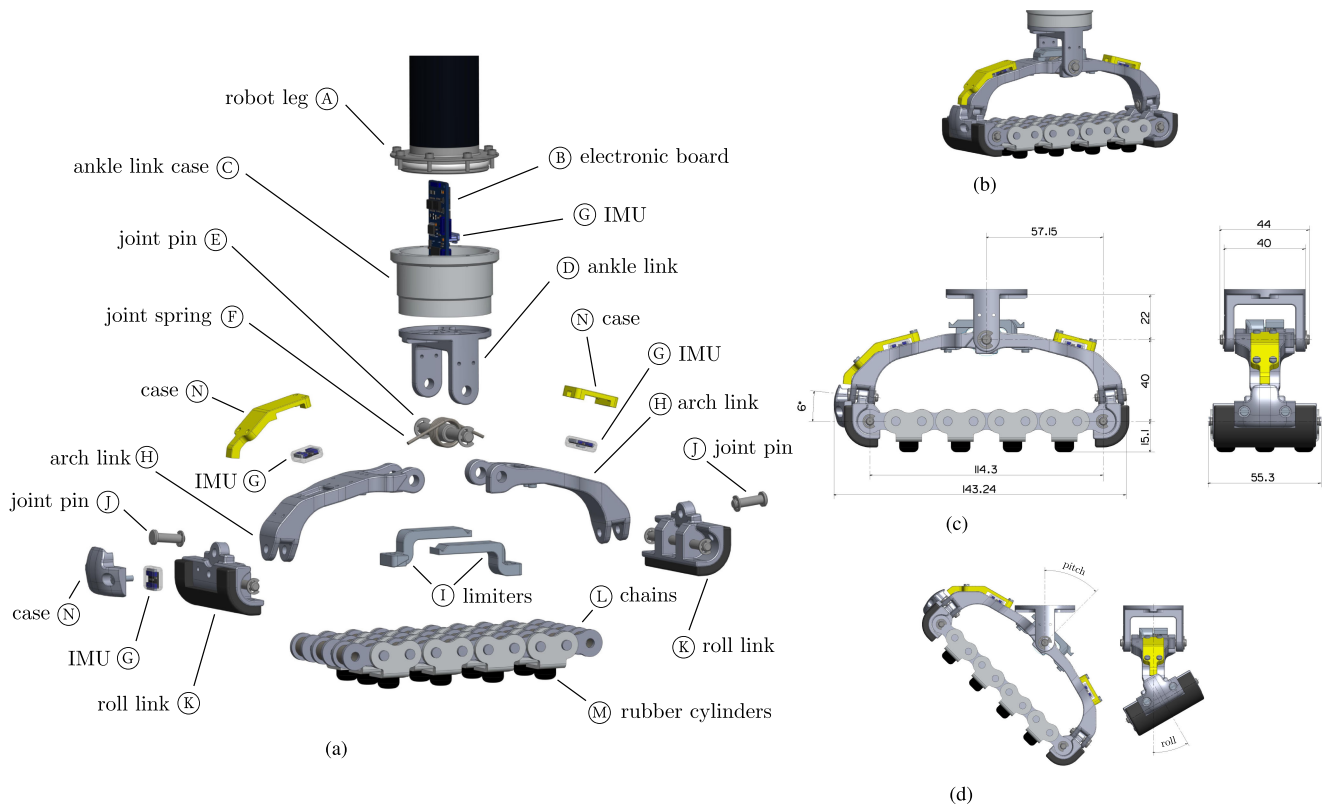
Fig. 5. (a) Exploded view of the SoftFoot-Q showing each of the relevant components of the foot. The placement of the electronic components (IMUs and custom board) of the sensing system are also shown. (b) Perspective. (c) Lateral and front. (d) CAD views of the mechanical design of SoftFoot-Q. The relevant dimensions (in mm) and angles of the parts of the prototypes are highlighted in the lateral and front views. (d) Pitch and roll motions of the foot.

foot also to variations of the profile of the terrain on the frontal plane.

## V. ADAPTIVE FEET: DESIGN

The required specifications for the design of SoftFoot-Q have been derived for its use on the quadrupedal robot ANYmal:[1] the size, mass, and inertia of the foot should be contained and compatible with the specifications of the robot; to reduce the sinkage of the foot in soft soil, the footprint should be maximized while keeping the weight low [45]; the adaptiveness in roll and pitch should be maximized avoiding any singularities in the range of motion of the joints; the sensing systems should be robust and accurate enough for the intended outdoor and indoor use.

The chosen design is shown as an exploded view in Fig. 5(a), while Fig. 5(b) and (c) depict perspective, lateral, and front views. SoftFoot-Q is composed of the following four main components.

1) An *ankle link* acts as the connecting component of the foot.

2) Two *arch links* provide the foot with pitching movements.
3) Two *roll links* make it possible to perform rotations around the forward axes.
4) Three *chains* are the core parts of SoftFoot-Q as they make the sole that deforms when coming into contact with an uneven terrain. The first three set of components are made of aluminium and the chains of stainless steel.

Referring to Fig. 5(a), the lower extremity Ⓐ of the leg of the quadruped is connected to the *ankle link* Ⓒ–Ⓓ, which in turn is attached to two *arch links* Ⓗ by means of a pin Ⓔ forming two revolute pitching joints. Using smaller pins Ⓙ, two links—called *roll links* Ⓚ—are joined to the extremities of the arch links opposite to the ankle link for providing the foot with rolling rotations. See Fig. 5(d) to better understand the two main types of movements that SoftFoot-Q can perform: roll joints provide a rotational degree of freedom to the sole on the frontal plane while pitch joints provide the same on the longitudinal plane. Additionally, the two arch links are connected to each other at the level of the pitching joints using also a spring Ⓕ for ensuring relative stiffness of the arch closure. Two limiters Ⓘ are also used to restrict the pitching angles: in their absence, the relative movement of the arch links could increase the pitch range of motion, which might cause the projection of the foot contact force to lie outside the support area, thus leading to instability of the foot. Finally, three paddled chains Ⓛ are attached to the front and back roll links, turning the foot into a closed kinematic
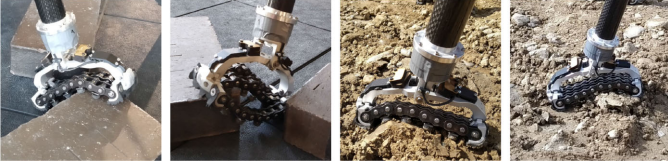
Fig. 6. Some examples of sole deformations and interactions while SoftFoot-Q engages different obstacles and terrains. Adaptability to the profile of the terrain is one of the main highlights of or foot.

chain and providing a flexible sole, which becomes rigid in extension. This enables the adaptiveness of the foot because, as it approaches an uneven terrain, the chains will move and conform to the terrain until the flexible sole becomes fully tense. Thus, the foot would envelop the convex hull of a subset of the points on the ground. The chains are also equipped with grousers with small rubber cylinders Ⓜ on part of the sole for increasing the grip on the ground. The relevant dimensions of the mechanical parts of the foot are reported in Fig. 5(c) and some more essential details are provided in Section VII in Table III. Also refer Appendix A for an analysis of the critical components of SoftFoot-Q. Fig. 6 shows some examples of feet deformations and interactions with different obstacles.

When the foot is at rest, the two roll axes of the foot are inclined approximately $6°$ upward with respect to the horizontal terrain plane [see Fig. 5(c)]. This choice is of extreme importance as it lets the foot sole to roll within a good range of foot poses. Here, one might argue that the movement of the roll links might get stuck whenever the two roll joint axes are not aligned. This is not the case with SoftFoot-Q, thanks to the play between the links of the chains. The inclination of $6°$ is justified by the fact that, through several tests, we found such particular value to be the average of all roll axes inclinations if the rest position of the axis were to be null.

The roll joint is positioned lower than the pitching one because a high position of the roll joint can seriously affect the stability of the foot by causing the projection of the force exerted by the leg to lie outside the support area (see Section III). As we were bound, by the required specifications, to keep the width of the sole limited for allowing continuous rotation of the shank of ANYmal, the only solution was to make the position of the roll joint as low as possible.

Fig. 5 also shows the sensing and perception components: four IMUs Ⓖ are placed on the feet in appropriate locations: one embedded in a custom electronic board Ⓑ mounted inside the ankle base, two on the upper part of the arch links, and one in front of the forward roll link. The positions of the IMUs on the foot are configured in such a way that there are always two sensors on the adjacent links of each joint of the foot except for the rear roll joint. This is by choice and for the sake of simplicity, since we assume for the time being that the two roll angles do not differ too much.

The IMUs we used on our foot are the Invensense MPU-9250 9-axis MEMS with gyroscope, accelerometer and magnetometer: in particular, the digital-output triple-axis gyroscope in the MPU-9250 has a user-programmable full scale range up to

$±2000$ deg/sec and an integrated low-pass filter; the digital-output triple-axis accelerometer has a programmable full scale range up to $±16\ g$. The sensors are made water resistant by coating them with an appropriate resin and by positioning them inside protective cases, such as Ⓝ, apart from the one inside the ankle. For more technical details about the IMUs, the reader may refer to the data-sheet of the Invensense MPU-9250 provided by the manufacturer.

The schematics of the custom electronic board, to which all IMUs are connected, are available openly at the GitHub page of Natural Machine Motion Initiative [51]. The PSoC firmware uploaded on the board handles readings from up to 17 connected IMUs. The communication with the board is established through FTDI and RS-485 protocols using a dedicated API. Each foot provides a USB cable, which can be attached to a hub to get measurement data from all feet. An ROS node [51] uses the aforementioned API to read and publish on a topic the accelerations and angular velocities of the IMUs connected to it at a maximum frequency of 200 Hz. The exact placements of each IMU on SoftFoot-Q are shown in Fig. 5.

## VI. POSE ESTIMATION AND HAPTIC EXPLORATION

### A. Pose Reconstruction

To employ SoftFoot-Q in harsh and hostile environments, it is highly desirable to know the pose of the foot to infer on characteristics (for instance, curvature or shape) of the surroundings with which the robot will be interacting (see also Section VI-B). However, the lack of joint encoders, which increases the robustness of SoftFoot-Q, makes it impossible to directly measure the joint angles.

We devised a simple foot pose reconstruction algorithm, which makes use of readings from the IMUs, for enhancing the perceptual capacities of the foot. It employs a complementary filter that fuses two estimates of the joint angles: one obtained through integration of angular velocities, measured by the gyroscopes, and the other from geometric considerations on the local gravity vector, acquired by the accelerometers.

The algorithm is based on the following assumptions.
1) The IMUs on each link are placed on the same locations and with the same orientation on all four feet.
2) The movements of the IMUs w.r.t. the related link bodies (changes in relative pose) are negligible.
3) The foot is not constantly subject to accelerations that are much greater than the acceleration of gravity.

For the sake of simplicity, consider the case of a single joint with two IMUs on the adjacent links (see Fig. 7). A preliminary estimate of the joint state $q_k^a$ (with joint axis $j_k$) can be obtained from the two accelerometers as the difference of the measurements of the gravity vectors from the rest position, as illustrated in Fig. 7

$$q_k^a = \theta_{k+1} - \theta_k. \qquad (9)$$

It is noteworthy that this estimate is purely based on geometric considerations and suffers severely in the cases where the gravity vector tends to align with the joint axis. Another estimate $q_k^g$ of the joint state can be integrated from the angular rate $\omega_k^g$ of the
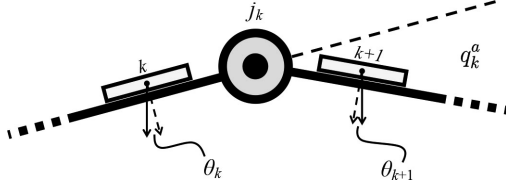
Fig. 7. Simple illustration of a revolute joint with two IMUs on the adjacent links. The variation of inclination of the gravity vectors measured by the two IMUs can give an estimate of the joint angle.

---

**Algorithm 1:** Angle Estimation of the $k$th Joint at $n$th Step.

1: **procedure** Joint States Estimation($a_k[n]$, $a_{k+1}[n]$, $\omega_k[n]$, $\omega_{k+1}[n]$, $q_k[n-1]$)

2: $\theta_k[n] = \dfrac{j_k \cdot (a_k[0] \times a_k[n])}{a_k[0] \cdot a_k[n]}$

3: $\theta_{k+1}[n] = \dfrac{j_k \cdot (a_{k+1}[0] \times a_{k+1}[n])}{a_{k+1}[0] \cdot a_{k+1}[n]}$

4: $q_k^a[n] = \theta_{k+1}[n] - \theta_k[n]$    ▷Acc. estimate

5: $\omega_k^g[n] = (\omega_{k+1}[n] - \omega_k[n]) \cdot j_k$

6: $q_k^g[n] = q_k[n-1] + \omega_k^g[n]\, dt$    ▷Gyro estimate

7: $q_k[n] = k_a q_k^a[n] + k_g q_k^g[n]$

8: **return** $q_k[n]$    ▷Joint angle estimate

---

joint, which in turn can be obtained trivially from the angular velocities of the two IMUs. This angle estimate is

$$q_k^g = q_k^* + \omega_k^g\, dt. \tag{10}$$

Here, $q_k^*$ is some reliable previous estimate of the joint angle. Fusing (9) and (10) with suitable weights, a complementary filter for the joint angle estimation can be defined as follows:

$$q_k[n] = k_a\, q_k^a[n] + k_g\, q_k^g[n]. \tag{11}$$

The variable $n$ stands for discrete time steps, the two positive gains $k_a$ and $k_g$ can be changed at each step $n$ according to the confidence in the two estimations ($q_k^a$ and $q_k^g$) and it should always hold that $k_a + k_g = 1$. In particular, we change the gains dynamically according to the degree of alignment of $j_k$ with the local gravity vector. Since the estimate $q_k^a$ is not reliable when $j_k$ is aligned with the local direction of the gravity, we set at each instant $k_g = |j_k \cdot a_k|$ and $k_a = 1 - k_g$.

From steps (9)–(11), an iterative procedure for estimating the joint angle between two links is devised (Algorithm 1). At the $n$th step, the Algorithm takes as input the acceleration vectors ($a_k[n]$ and $a_{k+1}[n]$), the angular velocity vectors ($\omega_k[n]$ and $\omega_{k+1}[n]$) of the two adjacent IMUs to the $k$th joint and the previous estimate of the joint angle $q_k[n-1]$ (to be used as initial condition $q_k^*$ for gyro integration). The output is an estimate of the joint angle $q_k[n]$. The procedure obviously needs to be applied for each joint of the robotic foot in order to reconstruct its entire pose.

The primary benefit of the complementary filter defined in (11) relies upon the fact that it is generally easier to implement on hardware than other more precise but complex solutions, such as a Kalman filter. Additionally, it does not suffer from yaw drift due to uncorrected integration of gyroscope measurements,



(a)       (b)


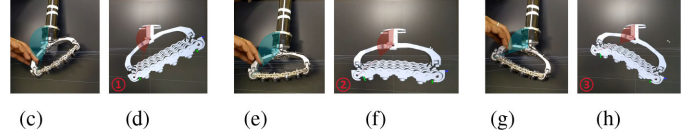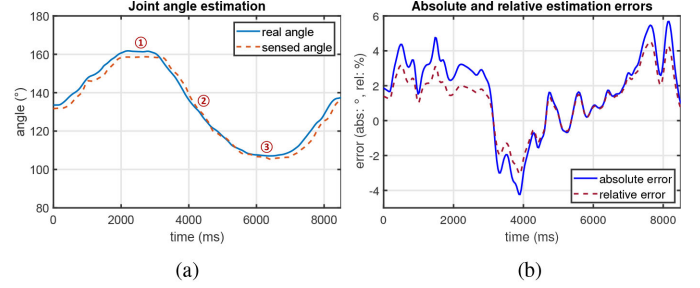
(c)    (d)    (e)    (f)    (g)    (h)

Fig. 8. Precision of the pose reconstruction algorithm (on a single joint of SoftFoot-Q) estimated by means of video tracking using Kinovea Software Suite. (a) Real and sensed angles. (b) Estimation errors. The feet poses in (c), (e), and (g) are estimated in (d), (f), and (h). These estimations are related to (a).



Fig. 9. Pose reconstruction of SoftFoot-Q on ANYmal. The shape of the foot is estimated by the software even under water.

which is common in traditional IMU-based orientation estimation, like the one proposed in [52]. The effort of implementation of our solution with respect to the accuracy it guarantees is sufficient for our application. Some additional processing of the sensor measurements with Low-Pass filters to clean up noise can further increase the precision.

The pose estimation algorithm was implemented in ROS Melodic and its accuracy was evaluated by using the built-in angle selection tool of the video tracking software suite Kinovea,[2] which provided the ground truth. This software suite is widely used in robotics research and achieves sufficient angle estimation accuracy in targets up to 5 m away [53]. An HD Canon camera was placed at a distance <1 m to record the videos and, additionally, also red colored dots where placed on the feet to better track the angles. The reconstruction was found to be responsive and precise for the intended use; for instance, we tested the estimation of the pitch angle and noticed relative errors on average smaller than 5% (with maximum absolute errors of $\approx \pm 6 \deg$ [see Fig. 8]). Three screenshots of the estimated poses and the real relative poses of the foot on ANYmal are shown in Fig. 9. These also show how the pose reconstruction is crucial wherever traditional sensing systems might fail. For instance, in the last photo of Fig. 9, notice that, even though a foot is submerged in muddy water, its configuration can still be sensed.
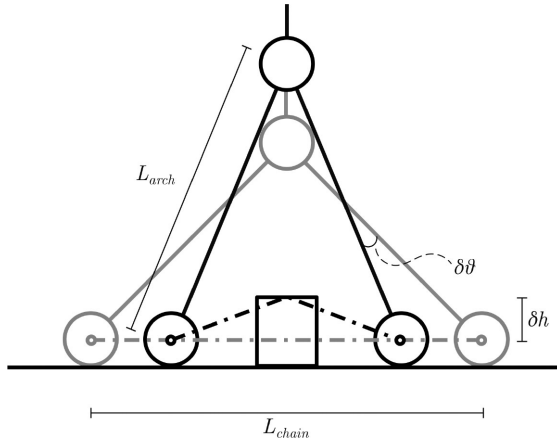
---

[2][Online]. Available: https://www.kinovea.org/

Fig. 10. Simplified qualitative resolution analysis of the smallest terrain profile variation that can be detected.

## B. Haptic Exploration

Tactile and haptic inspection with legged robots are relevant problems in the literature [44], [45], [54]. Indeed, using a purely visual inspection in places, such as deep underground mines or sewers, can lead to almost certain failures [55]. The sensing system can be employed for using SoftFoot-Q as a haptic probe to explore and sense the environment. This is in line with the aforementioned main advantage provided by robust adaptive feet, which is the possibility to have a more daring approach to the interaction process with the surroundings with the aim of increasing perceptual capabilities. For instance, one of the specifications on the foot design might be the ability to detect soil irregularities under the sole. The resolution with which we expect to sense irregularities can be approximately characterized mathematically.

Suppose a small obstacle at the center of the sole moves the chains upwards (see Fig. 10). From a simple and approximate geometric analysis, the following holds:

$$\delta\theta = 2\left[\arcsin\left(\frac{L_{chain}}{2L_{arch}}\right) - arcsin\left(\frac{\sqrt{\left(\frac{L_{chain}}{2}\right)^2 - \delta h^2}}{L_{arch}}\right)\right]. \tag{12}$$

Differentiating (12) with respect to $\delta h$ yields the sensitivity of the joint angle to variations in the height of the terrain profile
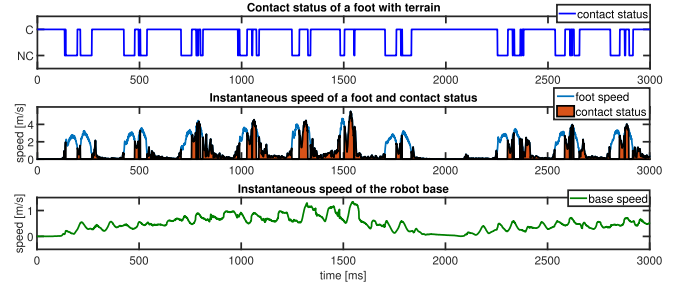
$$S = \frac{\partial(\delta\theta)}{\partial(\delta h)} = \frac{2\,\delta h}{L_{arch}\sqrt{1 - \frac{\frac{L_{chain}^2}{4} - \delta h^2}{L_{arch}^2}}\sqrt{\frac{L_{chain}^2}{4} - \delta h^2}}. \tag{13}$$
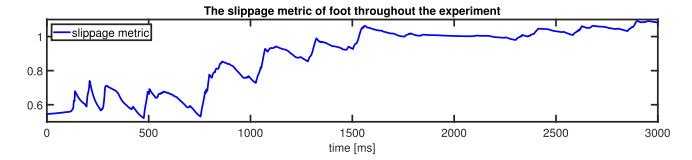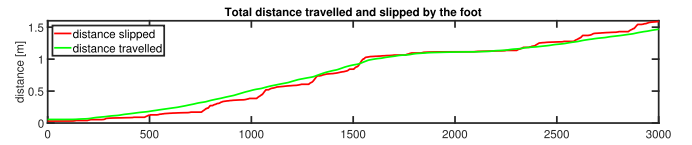
By inverting the relation in (12), we obtain

$$\delta h = \sqrt{\frac{L_{chain}^2}{4} - L_{arch}^2\sin\left(\frac{\delta\theta}{2} - \arcsin\left(\frac{L_{chain}}{2\,L_{arch}}\right)\right)^2} \tag{14}$$

which is approximately $14\,\mathrm{mm}$ in the case of SoftFoot-Q, if we take into account the worst case $\delta\theta = \pm6\,\mathrm{deg}$.

This type of irregularity detection is merely a simple illustrative example of the many possible applications of the



Fig. 11. Steps for the calculation of the slippage metric explained visually. For the sake of simplicity, only a single foot is considered. (a) Instantaneous speed of a foot and of the robot base, and the status of the contact of the foot with the ground. (b) Numerator (distance slipped by the foot) and denominator (distance travelled by the robot base) of the metric.

haptic perceptual capabilities of SoftFoot-Q. The real world applications of haptic perception and active exploration can range from inspection to search and rescue. The possibilities are innumerable since a sensorized adaptive foot can lead to an increased awareness about the geometry and properties of the environment. Empowering such an awareness would help the following:

1) in reducing the dependence on visual sensors, which are excessively influenced by natural variations;
2) in increasing locomotion stability by devising control techniques that explicitly make use of the information estimated via haptic exploration;
3) in opening new possibilities for industrial applications related to inspection.

## VII. EXPERIMENTAL VALIDATION

### A. Experimental Setup: Tests on ANYmal

This section presents the experimental data we collected, while testing SoftFoot-Q on the quadrupedal robot ANYmal [56] in order to show the effectiveness of the proposed prototype in enhancing the stability of the quadruped, its adaptiveness and robustness on uneven terrain (both in the field and indoors), and its ability in reducing slippage.

ANYmal weighs 30 kg and is approximately long 0.5 m; each of the four legs has three joints, which are driven by proprietary

series elastic actuators, called ANYdrives. These enable accurate control of locomotion. On-board batteries provide power to the robot for operating autonomously for more than 2 hours. The robot's underlying motion controller and additional software run on three on-board PCs.

During the experiments all relevant data were measured from both the feet and the robot: the state of the robot (base link position and orientation from the state estimator and the joint angles and torques of the legs) was recorded. Instead, the four SoftFoot-Qs provided measurements from the IMUs, which were used by Algorithm 1 for estimating the joint angles of the feet. During all experiments, both outdoor and indoor, no autonomy was used: the robot was commanded by an operator manually by giving velocity commands. The type of gaits that were used are mainly static walk and trot with an average velocity of the robot base of approximately 0.45 m/s.

Throughout both the outdoor and the indoor experiments, we measured and estimated the functional specifications that SoftFoot-Q complies with. The mechanical mobility, reliability under wet and varying temperature conditions, and the quality of sensing were also estimated and are reported in Table III.

### B. Outdoor Testing

Initially, extensive outdoor tests were performed by letting the robot walk on different terrains, mainly composed of mud, grass, and stones. Throughout the several testing sessions, in each experiment the average distance walked by ANYmal and the average speed were respectively about 10 m and 0.45 m/s. We also tested the performance of the feet on gentle slopes (inclination approximately less than 25%) as these could accentuate the phenomenon of slippage that we wish to minimize. We tested all three types of feet (ball, flat, and SoftFoot-Q), and the amount of slippage happening on the robotic legs was estimated.

While an accurate tracking of the robot utilizing external and fixed measuring devices would have been desirable, such an experimental setup is costly and was not available at the time we performed the tests. However, ANYmal features a state estimator that relies on the fusion of data coming from its perception system composed of IMUs, joint position, and torque sensors, and on the model of the robot [57], [58].

*1) Slippage Metric:* The state estimator of ANYmal outputs the poses of the tip points of the feet, their contact status and the motion of the base of the robot. From these estimates it is possible to assess the slippage of the feet to compare the performances of the different sets of feet quantitatively.

Let $C$ be the cartesian trajectory of the base reference frame of the robot and $C_i$ the cartesian trajectories of the feet (with $i = 1, 2, 3, 4$). $C_i^j$ will be the $j$th segment of $C_i$ considered only while it is in contact with the ground. By computing the distances $d_i^j$ and $d$ respectively along the trajectories $C_i^j$ and $C$, a metric

TABLE II
AVERAGE SLIPPAGE IN EXPERIMENTS

| | **Stones** | **Grass** | **Slope** | **Overall** |
|---|---|---|---|---|
| *Ball* [13] | 1.48 | 1.42 | 1.54 | 1.77 |
| *Flat* [46] | 1.83 | 2.53 | 1.91 | 2.09 |
| *SoftFoot-Q* | 1.37 | 1.28 | 1.25 | 1.36 |
| *Improvement (Ball-Soft) (%)* | 7.4 | 9.8 | 18.8 | 23.2 |
| *Improvement (Flat-Soft) (%)* | 25.1 | 49.4 | 34.5 | 34.9 |
| *Improvement (Average) (%)* | 16.25 | 29.6 | 26.65 | 29.05 |

can be expressed as follows:

$$m = \frac{\sum_i \sum_j d_i^j}{d}. \tag{15}$$

The numerator is the total distance traveled by all four feet while they are contacting the ground, whereas the denominator is the total distance traveled by the robot. Such a metric would have the following properties: it is null in the absence of slippage, larger when more slippage occurs, not affected by the length of the traveled path and by still phases, and, finally, it is only slightly affected by punctual events. However, particular attention must be devoted to comparing only similar runs since different gaits, speed, payload, and other parameters might affect the final metric value.

A series of graphs that can help understand the metric is shown in Fig. 11. Therein, for clarity of explanation, we consider the slippage of only one of the ball feet mounted on ANYmal during an outdoor experiment on slippery terrain. The first two plots of Fig. 11(a) show the status of the contact of the foot with the terrain and its instantaneous speed. The integral of the instantaneous speed of the foot over the time intervals, while it is contacting the terrain (area under the foot speed curve - highlighted in red), is the slippage, shown in red in the first plot of Fig. 11(b). On the other hand, the green curves show the instantaneous speed of the base frame of the robot and its integral (distance traveled by the robot). Finally, the slippage metric is plotted in blue in Fig. 11(b).

Results obtained for the outdoor tests using this metric are reported in Table II: it is possible to appraise an average reduction of slippage for SoftFoot-Q of about 29.05% for all the tests performed outdoors (in detail 16.25% on stones, 29.60% on collapsible terrain, 26.65% on slopes). It is noteworthy that the flat feet exhibited a marked tendency to slip, and a slower gait was required to properly perform the experiments. Despite the slower gait, the flat feet slipped more than the ball feet or SoftFoot-Qs. More testing was performed on mixed terrain that was partly muddy, covered with grass, and also having variable

Fig. 12.   Outdoor testing—Pictures show examples of the experimental setup. The first three images show the three feet on mixed grassy terrain. The last three show the same on stones. Slippage analysis is reported in Table II.

TABLE III
SUMMARY OF THE SPECIFICATIONS MET BY THE SOFTFOOT-Q

| | Description | Value |
|---|---|---|
| **Mechanical** | Weight of the foot | 0.420 kg |
| | Number of links per chain | 9 |
| | Weight of a single chain | 0.085 kg |
| | Weight of the sole | 0.255 kg |
| | Area of the footprint | $54 \times 143$ mm$^2$ |
| | Minimum curvature of foot sole | 27 mm |
| | Roll Range of Motion | $\pm 30$ deg |
| | Pitch Range of Motion | $\pm 45$ deg |
| | Minimum closure angle of foot arch | 40 deg |
| **Mobility** | Continuous rotation of the shank | -* |
| | Avg. speed - flat ground (over 2 m) | 0.7 m/s$^\dagger$ |
| | Avg. speed - flat slopes (over 2 m) | 0.4 m/s$^\dagger$ |
| | Avg. speed - uneven terrains (over 2 m) | 0.4 m/s$^\dagger$ |
| | Avg. speed - wet terrains (over 2 m) | 0.3 m/s$^\dagger$ |
| **Reliability** | Water and Dust protection | -* |
| | Normal thermal loads - min. range | $[0, 30]$ $^\circ C$ $^\ddagger$ |
| | Moderate thermal loads - min. range | $[-10, 40]$ $^\circ C$ $^\ddagger$ |
| | Mechanical loads - max. payload | 30 kg $^\dagger$ |
| | Mechanical loads - max. acc. | $3g$ $^\dagger$ |

*Verified through extensive outdoor and indoor experiments.
$^\dagger$Estimated from data harvested during experiments.
$^\ddagger$Estimated from data-sheet of components.

slopes (see Fig. 12): SoftFoot-Q performed better than both the ball and the flat feet in terms of slippage. By taking a global average of the slippage over all of the tests that were performed, the adaptive feet display lower slippage than the others (1.36 for adaptive, 1.77 for ball, and 2.09 for flat feet), hence an improvement of 23.2% with respect to ball feet and of 34.9% relative to flat feet.

During the experiments we noticed that our feet performed particularly well on soft terrain, especially on sand, grass, and mud. We were also able to walk the robot on water puddles and dusty areas without damaging the electronics of SoftFoot-Q. At the end of the experiments, even though
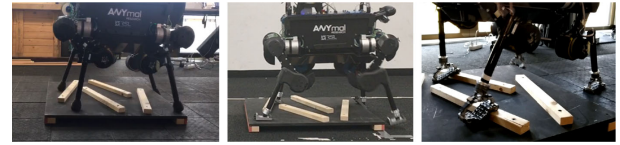


Fig. 13.   Indoor testing—Setup used for evaluating the slippage in controlled environment with ball feet, flat feet, and adaptive feet.

we used the same four feet for all the tests (both the indoor and the very harsh outdoor ones), no significant electrical or mechanical damage was reported, and any accumulated dirt or mud did not hinder operation. Moreover, the use of SoftFoot-Q did not require any alteration of the speed of the robot: neither any significant increase nor any reduction were seen during the experiments (see attached submission video).

*C. Indoor Testing*

Additionally, indoor tests were also performed by letting the robot walk forward and backward on a platform composed of fixed rectangular beams. Using each foot, the same distance was covered (from one side of the platform to the other). We manually commanded the robot to maintain the same speed. The platform was big enough for ANYmal to stand with all four legs on it: the dimensions were approximately $150 \times 120 \times 7 \, \text{cm}^3$. The four beams on the platform had a profile of approximate dimensions $3 \times 2 \, \text{cm}^2$, and were placed at random angles in order to increase uncertainty during the tests. These indoor experiments allowed us to evaluate the performance of the feet in a controlled environment through repeatable experiments, which were conducted with ball, flat and adaptable feet, as shown in Fig. 13.

A different criterion (visual inspection in place of the slippage metric used for outdoor tests) was purposely employed here since we wanted to measure the phenomena of instantaneous and sudden slippages instead of an aggregate measure. The sudden downward movement of a foot, which is caused by the robot losing a foothold, might not always induce instability of the robot itself and might not always be crucial for operation. However, it can give an indication of the grip and the reduced slippage that our foot design can ensure. Depending on the terrain and the situation, these type of slips can be more or less critical for locomotion.

A simple visual analysis of slippage was carried out by counting the number of times the robot legs slipped from an expected foothold. A slippage was counted for whenever a leg
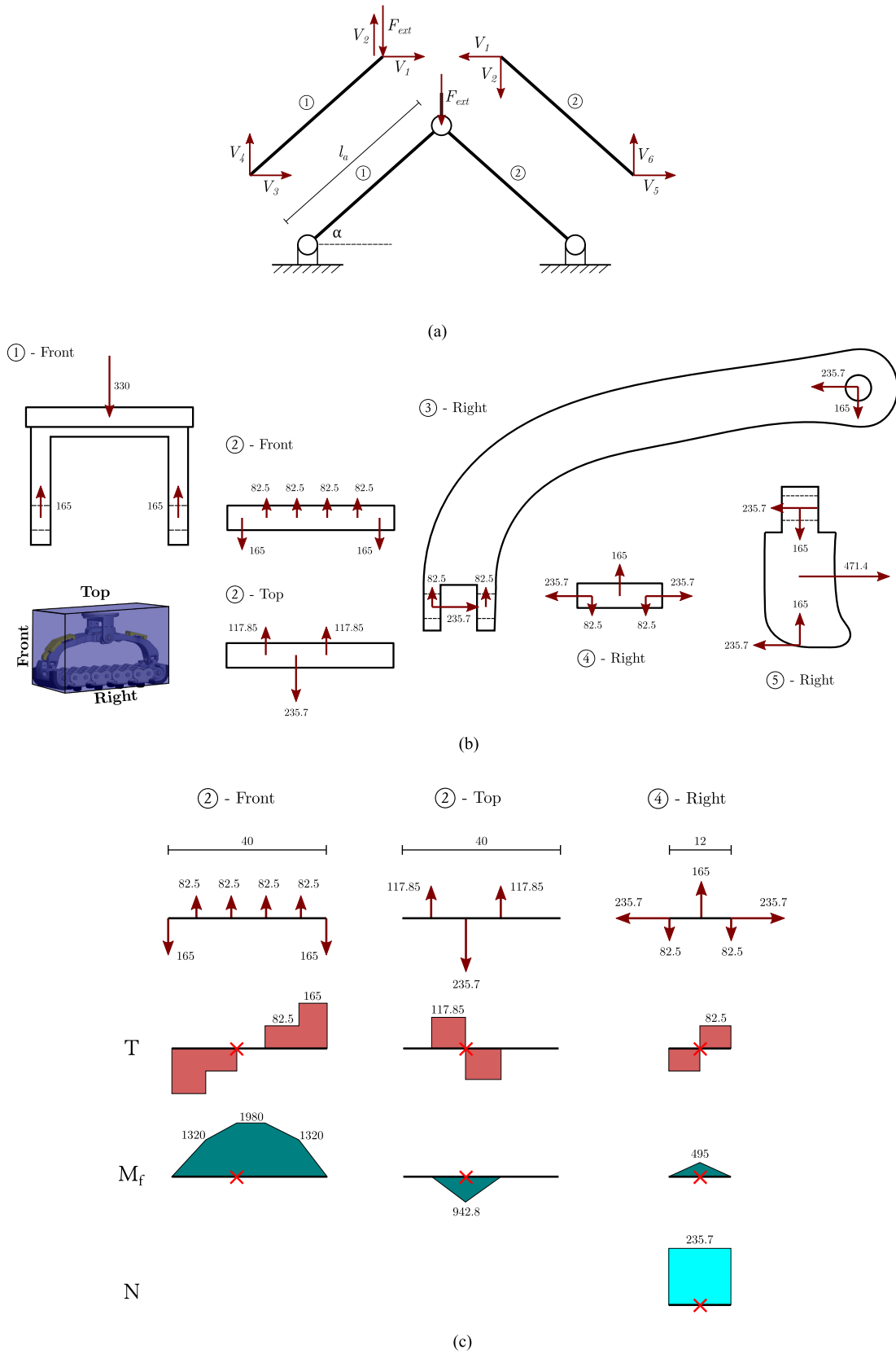
Fig. 14. Simplified load bearing analysis of the critical components of SoftFoot-Q: the pitch and roll joint pins. The von Mises equivalent tensile stress of the two pins are $\sigma_{VM}^{(p)} = 179.46$ MPa and $\sigma_{VM}^{(r)} = 97.94$ MPa.

lost the expected foothold with a sudden downward movement of the foot and a velocity of the tip of the leg much higher than its average speed throughout the test (see attached submission video). Since the total number of steps taken by the robot were different for each foot, we normalized the number of slips by the count of steps taken. We noticed a significantly lower percentage of slippage in the case of our adaptive feet with respect to ball and flat feet (4.0% versus 8.0% and 16.2%) on an average of 100 steps walked by the robot.

## VIII. Conclusion

In this work, we presented the SoftFoot-Q, a novel adaptive foot, devised with the particular goal of being used on quadrupedal robots. Our prior work [11] loosely inspired this prototype, which preserved all of the advantages of adaptiveness and robustness of the previous foot. Furthermore, SoftFoot-Q was specifically designed for quadrupedal navigation in outdoor terrain and mud. It was more adaptive, robust, light, and simple than its predecessor. The proposed robotic foot also tried to overcome the limitations of current feet as its core functioning principle was to conform to the shape of the ground so as to attempt to maximize the contact surface, and thus, stabilized the quadrupedal walker by reducing feet slippage. A summary of the mechanical and functional requirements that the SoftFoot-Q complies with, were shown in Table III.

We started by discussing and proving mathematically some of the limitations that affected traditional ball and flat feet, which were commonly used on quadrupeds. These were substantial, especially when they were used for walking outdoors on uneven and unstructured terrain or on slopes and, in general, wherever the knowledge about the profile of the ground was imperfect. This analysis led us to the choice of design as it proved that a mechanically adaptive sole was inherently stable even in the absence of frictional phenomena.

After describing in detail the chosen adaptive foot design and its low-cost but effective sensing system composed of inertial measurement units, we implemented a computationally efficient and precise algorithm for foot pose reconstruction. Further work is currently being carried out for estimating other relevant quantities, such as contact forces during locomotion, which can provide additional information about the interaction of the foot with the environment.

The effectiveness of SoftFoot-Q was validated through extensive in-field testing: the adaptive feet were mounted on a compliantly actuated quadrupedal robot and compared with the traditional counterparts, ball and flat feet, on harsh irregular terrain with different softness and consistency. Results showed a performance improvement measured in terms of slippage. Surprisingly, the flat feet displayed more instability during the tests than did the ball feet. Furthermore, these experiments also proved the robustness and adaptiveness of the proposed prototype. Additionally, indoor tests were also conducted; the total number of times the robot slipped was visually estimated for each of the trials. Outcomes display a reduced number of slips of the robot while mounting the SoftFoot-Q, whereas ball and flat feet slipped much more during locomotion.

In conclusion, our foot design was clearly seen to improve the stability of quadrupeds by reducing slippage considerably during locomotion without any need of slowing down the robot. The sensing module and the pose reconstruction algorithm are a good point of departure for enhancing the haptic feedback of the probe. Future works might include designing an actuated version of the foot to actively stabilize quadrupedal robots and devising control algorithms that make use of the information provided by SoftFoot-Q to improve locomotion. Also the design of the proposed foot will be further improved by investigating the option of efficiently adapting it to different robots and of adding elasticity to the ankle.

## Appendix

### A. Load Bearing Analysis

A simplified load bearing analysis (see Fig. 14) was performed in order to prove the robustness of the prototype. In particular, stress analysis of the two critical components of the foot (the joint pins) was carried out. We used the data saved during the experiments to find the highest possible load on the feet ankles, which is $F_{ext} \approx 330\,\mathrm{N}$.

Subsequently, a reduced model [see Fig. 14(a)] on the longitudinal plane was employed to compute the reactions of the joint pins to such a load. These aided in drawing the free body diagrams [see Fig. 14(b)] of each of the main components of SoftFoot-Q, considering also the longitudinal symmetry of the foot and some minor simplifying assumptions.

Finally, the stress analysis of the two joint pins of the foot were performed [see Fig. 14(c)] and the von Mises criterion was used to evaluate their yielding. For the pitch joint pin we computed an equivalent tensile stress of $\sigma_{VM}^{(p)} = 179.46\,\mathrm{MPa}$. Instead, the roll joint pin had $\sigma_{VM}^{(r)} = 97.94\,\mathrm{MPa}$. Both values are fairly below the yield strength of stainless steel (pins are made of EN 1.4301), which is greater than $200\,\mathrm{MPa}$.

## References

[1] N. B. Ignell, N. Rasmusson, and J. Matsson, "An overview of legged and wheeled robotic locomotion," in *Proc. Mini-Conf. Interesting Results Comput. Sci. Eng.*, vol. 21, 2012.

[2] D. Torricelli *et al.*, "Human-like compliant locomotion: State of the art of robotic implementations," *Bioinspiration Biomimetics*, vol. 11, no. 5, 2016, Art. no. 051002.

[3] D. M. Bramble and D. E. Lieberman, "Endurance running and the evolution of homo," *Nature*, vol. 432, no. 7015, pp. 345–352, 2004.

[4] M. Venkadesan, M. M. Bandi, and S. Mandre, *Biological Feet: Evolution, Mechanics and Applications*. New York, NY, USA: Elsevier, 2017.

[5] J. Bares *et al.*, "Ambler: An autonomous rover for planetary exploration," *Computer*, vol. 22, no. 6, pp. 18–26, 1989.

[6] E. M. Hennig and T. Sterzing, "Sensitivity mapping of the human foot: Thresholds at 30 skin locations," *Foot Ankle Int.*, vol. 30, no. 10, pp. 986–991, 2009.

[7] H. M. Herr and A. M. Grabowski, "Bionic ankle-foot prosthesis normalizes walking gait for persons with leg amputation," in *Proc. Roy. Soc. London B: Biol. Sci.*, vol. 279, no. 1728, pp. 457–464, 2012.

[8] D. Hill and H. Herr, "Effects of a powered ankle-foot prosthesis on kinetic loading of the contralateral limb: A case series," in *Proc. IEEE Int. Conf. Rehabil. Robot.*, 2013, pp. 1–6.

[9] B. Brackx, M. Van Damme, A. Matthys, B. Vanderborght, and D. Lefeber, "Passive ankle-foot prosthesis prototype with extended push-off," *Int. J. Adv. Robot. Syst*, vol. 10, no. 2, p. 101, 2013, doi: 10.5772/55170.

[10] P. Cherelle, V. Grosu, M. Cestari, B. Vanderborght, and D. Lefeber, "The amp-foot 3, new generation propulsive prosthetic feet with explosive motion characteristics: Design and validation," *Biomed. Eng. online*, vol. 15, no. 3, 2016, Art. no. 145.

[11] C. Piazza *et al.*, "Toward an adaptive foot for natural walking," in *Proc. IEEE-RAS Int. Conf. Humanoid Robots (Humanoids)*, 2016, pp. 1204–1210. [Online]. Available: http://ieeexplore.ieee.org/document/7803423/

[12] M. G. Catalano *et al.*, "HRP-4 walks on soft feet," *IEEE Robot. Autom. Lett.*, vol. 6, no. 2, pp. 470–477, Apr. 2020.

[13] M. Hutter *et al.*, "Anymal - toward legged robots for harsh environments," *Adv. Robot.*, vol. 31, no. 17, pp. 918–931, 2017. [Online]. Available: https://doi.org/10.1080/01691864.2017.1378591

[14] "Boston Dynamics Website," 2017, Accessed: Mar. 1, 2017. [Online]. Available: http://www.bostondynamics.com

[15] "Agility Robotics Unveils Upgraded Digit Walking Robot," 2019. [Online]. Available: https://spectrum.ieee.org/automaton/robotics/humanoids/agility-robotics-digit-v2-biped-robot

[16] K. Kaneko, K. Harada, F. Kanehiro, G. Miyamori, and K. Akachi, "Humanoid robot HRP-3," in *Proc. IEEE/RSJ Int. Conf. Intell. Robots Syst.*, 2008, pp. 2471–2478.

[17] I.-W. Park, J.-Y. Kim, J. Lee, and J.-H. Oh, "Mechanical design of humanoid robot platform KHR-3 (KAIST humanoid robot 3: Hubo)," in *Proc. 5th IEEE-RAS Int. Conf. Humanoid Robots*, 2005, pp. 321–326.

[18] D. Gouaillier *et al.*, "Mechatronic design of NAO humanoid," in *Proc. IEEE Int. Conf. Robot. Autom.*, 2009, pp. 769–774.

[19] O. Stasse *et al.*, "Talos: A new humanoid research platform targeted for industrial applications," in *Proc. IEEE-RAS 17th Int. Conf. Humanoid Robot. (Humanoids)*, 2017, pp. 689–695.

[20] J. Englsberger *et al.*, "Overview of the torque-controlled humanoid robot Toro," in *Proc. IEEE-RAS Int. Conf. Humanoid Robots*, 2014, pp. 916–923.

[21] F. Negrello *et al.*, "Walk-man humanoid lower body design optimization for enhanced physical performance," in *Proc. IEEE Int. Conf. Robot. Autom.*, 2016, pp. 1817–1824.

[22] D. Kim, Y. Zhao, G. Thomas, B. R. Fernandez, and L. Sentis, "Stabilizing series-elastic point-foot bipeds using whole-body operational space control," *IEEE Trans. Robot.*, vol. 32, no. 6, pp. 1362–1379, Dec. 2016.

[23] J. W. Grizzle, J. Hurst, B. Morris, H.-W. Park, and K. Sreenath, "Mabel, a new robotic bipedal walker and runner," in *Proc. IEEE Amer. Control Conf.*, 2009, pp. 2030–2036.

[24] "This Robot Ostrich Can Ride Around on Hovershoes," 2017. [Online]. Available: https://spectrum.ieee.org/automaton/robotics/robotics-hardware/cassie-on-hovershoes

[25] D. Kim, S. J. Jorgensen, J. Lee, J. Ahn, J. Luo, and L. Sentis, "Dynamic locomotion for passive-ankle biped robots and humanoids using whole-body locomotion control," *Int. J. Robot. Res.*, vol. 39, no. 8, pp. 936–956, 2020.

[26] C. Semini, N. G. Tsagarakis, E. Guglielmino, M. Focchi, F. Cannella, and D. G. Caldwell, "Design of HYQ-a hydraulically and electrically actuated quadruped robot," in *Proc. Institution Mech. Eng., Part I: J. Syst. Control Eng.*, vol. 225, no. 6, pp. 831–849, 2011.

[27] "This Robotics Startup Wants to Be the Boston Dynamics of China," 2017. [Online]. Available: https://spectrum.ieee.org/automaton/robotics/robotics-hardware/this-robotics-startup-wants-to-be-the-boston-dynamics-of-china

[28] G. Bledt, M. J. Powell, B. Katz, J. Di Carlo, P. M. Wensing, and S. Kim, "MIT Cheetah 3: Design and control of a robust, dynamic quadruped robot," in *Proc. IEEE/RSJ Int. Conf. Intell. Robots Syst.*, 2018, pp. 2245–2252.

[29] "Boston Dynamics Spotmini is All Electric, Agile, and Has a Capable Face-Arm. 2016. [Online]. Available: http://spectrum.ieee.org/automaton/robotics/home-robots/boston-dynamics-spotmini

[30] J. Li, Q. Huang, W. Zhang, Z. Yu, and K. Li, "Flexible foot design for a humanoid robot," in *Proc. IEEE Int. Conf. Autom. Logistics*, 2008, pp. 1414–1419.

[31] N. G. Tsagarakis, Z. Li, J. Saglia, and D. G. Caldwell, "The design of the lower body of the compliant humanoid robot 'cCub'," in *Proc. IEEE Int. Conf. Robot. Autom.*, 2011, pp. 2035–2040.

[32] A. Najmuddin, Y. Fukuoka, and S. Ochiai, "Experimental development of stiffness adjustable foot sole for use by bipedal robots walking on uneven terrain," in *Proc. IEEE/SICE Int. Symp.*, 2012, pp. 248–253.

[33] R. Käslin, H. Kolvenbach, L. Paez, K. Lika, and M. Hutter, "Towards a passive adaptive planar foot with ground orientation and contact force sensing for legged robots," in *Proc. IEEE/RSJ Int. Conf. Intell. Robot. Syst.*, Oct. 2018, pp. 2707–2714.

[34] S. Davis and D. G. Caldwell, "The design of an anthropomorphic dexterous humanoid foot," in *Proc. IEEE/RSJ Int. Conf. Intell. Robot. Syst.*, 2010, pp. 2200–2205.

[35] H.-J. Kang *et al.*, "Realization of biped walking on uneven terrain by new foot mechanism capable of detecting ground surface," in *Proc. IEEE Int. Conf. Robot. Autom.*, 2010, pp. 5167–5172.

[36] D. Kuehn *et al.*, "Active spine and feet with increased sensing capabilities for walking robots," in *Proc. Int. Symp. Artif. Intell. Robot. Autom. Space*, 2012, pp. 4–6.

[37] S. Hauser, P. Eckert, A. Tuleu, and A. Ijspeert, "Friction and damping of a compliant foot based on granular jamming for legged robots," in *Proc. IEEE RAS-EMBS Int. Conf. Biomed. Robot. Biomechatronics,* 2016, pp. 1160–1165.

[38] L. Paez, K. Melo, R. Thandiackal, and A. J. Ijspeert, "Adaptive compliant foot design for salamander robots," in *Proc. 2nd IEEE Int. Conf. Soft Robot.*, 2019, pp. 178–185.

[39] J.-T. Seo and B.-J. Yi, "Modeling and analysis of a biomimetic foot mechanism," in *Proc. IEEE/RSJ Int. Conf. Intell. Robot. Syst.*, 2009, pp. 1472–1477.

[40] L. Colasanto, N. Van der Noot, and A. J. Ijspeert, "Bio-inspired walking for humanoid robots using feet with human-like compliance and neuromuscular control," in *Proc. IEEE-RAS 15th Int. Conf. Humanoid Robots (Humanoids)*, 2015, pp. 26–32.

[41] A. Kalamdani, C. Messom, and M. Siegel, "Robots with sensitive feet," *IEEE Instrum. Meas. Mag.*, vol. 10, no. 5, pp. 46–53, Oct. 2007.

[42] D. Kuehn *et al.*, "Additional DoFs and sensors for bio-inspired locomotion: Towards active spine, ankle joints, and feet for a quadruped robot," in *Proc. Int. Conf. Robot. Biomimetics.*, 2011, pp. 2780–2786.

[43] E. R. Westervelt, J. W. Grizzle, C. Chevallereau, J. H. Choi, and B. Morris, *Feedback Control of Dynamic Bipedal Robot Locomotion*. Boca Raton, FL, USA: CRC Press, 2007, vol. 28.

[44] H. Kolvenbach, G. Valsecchi, R. Grandia, A. Ruiz, F. Jenelten, and M. Hutter, "Tactile inspection of concrete deterioration in sewers with legged robots," in *Proc. 12th Conf. Field Service Robot.*, 2019.

[45] H. Kolvenbach, C. Bärtschi, L. Wellhausen, R. Grandia, and M. Hutter, "Haptic inspection of planetary soils with legged robots," *IEEE Robot. Autom. Lett.*, vol. 4, no. 2, pp. 1626–1632, Apr. 2019.

[46] G. Valsecchi, R. Grandia, and M. Hutter, "Quadrupedal locomotion on uneven terrain with sensorized feet," *IEEE Robot. Autom. Lett.*, vol. 5, no. 2, pp. 1548–1555, Apr. 2020.

[47] M. Kalakrishnan, J. Buchli, P. Pastor, M. Mistry, and S. Schaal, "Learning, planning, and control for quadruped locomotion over challenging terrain," *Int. J. Robot. Res.*, vol. 30, no. 2, pp. 236–258, 2011.

[48] A. S. Voloshina, A. D. Kuo, M. A. Daley, and D. P. Ferris, "Biomechanics and energetics of walking on uneven terrain," *J. Exp. Biol.*, vol. 216, no. 21, pp. 3963–3970, 2013.

[49] R. Mengacci, F. Angelini, M. G. Catalano, G. Grioli, A. Bicchi, and M. Garabini, "Stiffness bounds for resilient and stable physical interaction of articulated soft robots," *IEEE Robot. Autom. Lett.*, vol. 4, no. 4, pp. 4131–4138, Oct. 2019.

[50] E. A. Fuller, "The windlass mechanism of the foot. A mechanical model to explain pathology," *J. Amer. Podiatric Med. Assoc.*, vol. 90, no. 1, pp. 35–46, 2000.

[51] NMMI, *Natural Machine Motion Initiative - Github*, 2019. [Online]. Available: https://github.com/NMMI

[52] G. Santaera, E. Luberto, A. Serio, M. Gabiccini, and A. Bicchi, "Low-cost, fast and accurate reconstruction of robotic and human postures via IMU measurements," in *Proc. IEEE Int. Conf. Robot. Autom.*, 2015, pp. 2728–2735.

[53] A. Puig-Diví, C. Escalona-Marfil, J. M. Padullés-Riu, A. Busquets, X. Padullés-Chando, and D. Marcos-Ruiz, "Validity and reliability of the Kinovea program in obtaining angles and distances using coordinates in 4 perspectives," *PLoS One*, vol. 14, no. 6, 2019, Art. no. e0216448.

[54] H. Kolvenbach *et al.*, "Towards autonomous inspection of concrete deterioration in sewers with legged robots," *J. Field Robot.*, vol. 37, no. 8, pp. 1314–1327, 2020.

[55] R. Zimroz, M. Hutter, M. Mistry, P. Stefaniak, K. Walas, and J. Wodecki, "Why should inspection robots be used in deep underground mines?" in *Proc. 27th Int. Symp. Mine Plan. Equip. Selection*, 2019, pp. 497–507.

[56] M. Hutter *et al.*, "ANYmal - a highly mobile and dynamic quadrupedal robot," in *Proc. IEEE/RSJ Int. Conf. Intell. Robot. Syst.*, 2016, pp. 38–44. [Online]. Available: http://ieeexplore.ieee.org/document/7758092/

[57] M. Bloesch, C. Gehring, P. Fankhauser, M. Hutter, M. A. Hoepflinger, and R. Siegwart, "State estimation for legged robots on unstable and slippery terrain," in *Proc. IEEE/RSJ Int. Conf. Intell. Robot. Syst.*, 2013, pp. 6058–6064.

[58] M. Bloesch *et al.*, "State estimation for legged robots-consistent fusion of leg kinematics and IMU," *Robotics*, vol. 17, pp. 17–24, 2013.

**Manuel Giuseppe Catalano** received the B.S. and M.S. degrees in mechanical engineering and the Ph.D. degree in robotics from the University of Pisa, Pisa, Italy, in 2006, 2008, and 2013, respectively.

He is currently a Researcher with the Italian Institute of Technology, Genoa, Italy, and a collaborator of the Research Center "E. Piaggio," University of Pisa. His research interests include the design of soft robotic systems, human "robot interaction, and prosthetics.

Dr. Catalano was the recipient of the Georges Giralt Ph.D. Award in 2014, the prestigious annual European award given for the best Ph.D. thesis by euRobotics AISBL.



**Mathew Jose Pollayil** received the B.S. degree in biomedical engineering and the M.S. degree (cum laude) in robotics and automation engineering from the University of Pisa, Pisa, Italy, where he is currently working toward the Ph.D. degree in robotics with the Research Center "E. Piaggio" and with the Dipartimento di Ingegneria dell–Informazione.

He is an Affiliated Researcher with the Italian Institute of Technology, Genova, Italy. His main research interests include nonlinear control and planning quadrupedal locomotion.



**Giorgio Grioli** received the Ph.D. degree in robotics, automation, and engineering from the University di Pisa, Pisa, Italy, in 2011.

He is a Researcher with the Italian Institute of Technology, Genova, Italy, investigates the design, modeling, and control of soft robotics systems applied to augmentation of, rehabilitation of and interaction with the human. He authored more than 80 journal articles, conference articles, and book chapters (2200 citations, h-index 20). He is reported as inventor in six between patent and patent applications. He contributed to the development of several robotic systems and to the founding of a spin-off company. His research interest includes collaborative industrial robotics to prosthetics.



**Giorgio Valsecchi** received the master's degree in aerospace and industrial engineering from the Scuola Superiore Sant'Anna, Pisa, Italy, and Pisa University, Pisa, in 2017. He is currently working toward the Ph.D. degree in mechanical and process engineering with Robotic Systems Lab., ETH Zurich, Zurich, Switzerland.

After graduating, he spent two years working on robotics solutions for civil and industrial infrastructure inspection. His research interests include the design of robots for extreme environments, mobility concepts, and novel mechanisms.



**Hendrik Kolvenbach** received the B.Sc. and M.Sc. degree in mechanical engineering from RWTH Aachen University, Aachen, Germany, in 2013 and 2014, respectively.

After a training period with the European Space Agency from 2014 to 2016, he joined the Robotic Systems Lab, ETH Zurich, Zurich, Switzerland, to pursue a doctoral degree. His research interests include robotic system design and the application of legged systems for planetary exploration.



**Marco Hutter** received the Ph.D. degree in mechanical engineering from the ETH Zurich, Zurich, Switzerland. He is an Assistant Professor for Robotic Systems with ETH Zurich, Zurich, Switzerland. Marco is part of the National Centre of Competence in Research (NCCR) Robotics and NCCR Digital Fabrication and PI in various international projects (e.g., EU Thing) and challenges (e.g., DARPA SubT). His research interests include the development of novel machines and actuation concepts together with the underlying control, planning, and machine learning algorithms for locomotion and manipulation.

Prof. Hutter's work has been recognized with a number of awards and prestigious grants such as the Branco Weiss Fellowship, ETH medal, IEEE/RAS Early Career Award or ERC Starting Grant.



**Antonio Bicchi** received the Ph.D. degree in mechanical engineering from the University of Bologna, Bologna, Italy. He is a Scientist interested in robotics and intelligent machines.

He holds a chair in Robotics with the University of Pisa, Pisa, Italy, and leads the Soft Robotics Laboratory, Italian Institute of Technology, Genova, Italy. He is also an Adjunct Professor with Arizona State University, Tempe, USA. His work has been recognized with many international awards and has earned him four prestigious grants from the European Research Council (ERC). He launched initiatives such as the WorldHaptics conference series, the IEEE Robotics and Automation Letters, and the Italian Institute of Robotics and Intelligent Machines.



**Manolo Garabini** received the M.S. degree in mechanical engineering and the Ph.D. degree in robotics from the University of Pisa, Pisa, Italy.

He is currently an Assistant Professor with the University of Pisa. A part of his activity has been devoted to theoretically demonstrate the effectiveness of soft and adaptive robots in high performance, high efficiency and resilient tasks via analytical and numerical optimization tools. He contributed to the realization of modular Variable Stiffness Actuators. He contributed in the design of the joints and the lower body of the humanoid robot WALK-MAN and took part at the DARPA Robotics Challenge and at a field test in Amatrice, Italy after a disastrous earthquake event. Recently he contributed to the development of an efficient and effective compliance planning algorithms for interaction under uncertainties. Currently, he is the Principal Investigator with the THING H2020 EU Research Project for the University of Pisa, and the coordinator of the Dysturbance H2020 Eurobench sub-project and NI H2020 EU Research Project. His main research interests include the design, planning and control of soft and adaptive robots, from single joints, to end-effectors (hands, grippers, feet), to complex systems.